(This is a sample cover image for this issue. The actual cover is not yet available at this time.)

Earth and Planetary Science Letters 362 (2013) 88–98

Contents lists available at SciVerse ScienceDirect

Earth and Planetary Science Letters

journal homepage: www.elsevier.com/locate/epsl

Andean-scale highlands in the Late Cretaceous Cordillera of the North American western margin

Jacob O. Sewall [a,*], Henry C. Fricke [b]

[a] Department of Physical Sciences, Kutztown University, Kutztown, PA 19530, USA
[b] Department of Geology, Colorado College, Colorado Springs, CO 80903, USA

ARTICLE INFO

Article history:
Received 5 January 2012
Received in revised form
20 November 2012
Accepted 1 December 2012
Editor: J. Lynch-Stieglitz

Keywords:
North American Cordillera
paleoelevation
Campanian
Sevier
Cretaceous
climate modeling

ABSTRACT

From the Late Jurassic through the Cretaceous, collision between the North American and Farallon plates drove extensive thin-skinned thrusting and crustal shortening that resulted in substantial relief in the North American Cordillera. The elevation history of this region is tightly linked to the tectonic, climatic and landscape evolution of western North America but is not well constrained. Here we use an atmospheric general circulation model with integrated oxygen isotope tracers (isoCAM3) to predict how isotope ratios of precipitation would change along the North American Cordillera as the mean elevation of orogenic highlands increased from 1200 m to 3975 m. With increases in mean elevation, highland temperatures fall, monsoonal circulation along the eastern front of the Cordillera is enhanced, and wet season (generally spring and summer) precipitation increases. Simulated oxygen isotopic ratios in that precipitation are compared to those obtained from geologic materials (e.g. fossil bivalves, authigenic minerals). Quantification of match between model and data-derived $\delta^{18}O$ values suggests that during the Late Cretaceous, the best approximation of regional paleoelevation in western North America is a large orogen on the scale of the modern Andes Mountains with a mean elevation approaching 4000 m and a north-south extent of at least 15° of latitude.

1. Introduction

Throughout the Cretaceous, subduction of the Farallon plate under North America drove broad regional folding and thrusting in the western craton (DeCelles, 2004). This prolonged deformational event is termed the Sevier orogeny; it was characterized by crustal shortening of up to 75% (DeCelles and Coogan, 2006) and produced north-south trending structures and topography along the western margin of North America from Alaska to Mexico (DeCelles, 2004). By the Campanian (~75 Ma), fluvial transport and deposition of sediments from the growing orogeny had resulted in extensive foreland basin filling and development of a broad, low-relief coastal plain separating the highlands in the west from the Western Interior Seaway to the east (Aschoff and Steel, 2011; DeCelles, 2004; Roberts and Kirschbaum, 1995; Fig. 1).

While the deformation style, regional extent and horizontal translation of crustal material in the Cordilleran (Sevier) fold and thrust belt are relatively well documented (e.g. Burchfiel and Davis, 1972; Currie, 2002; DeCelles and Coogan, 2006; DeCelles, 2004; Elison; 1991; Friedrich and Bartley, 2003; Hudec and Davis, 1989; Weil et al., 2010), the actual elevation of the resulting Campanian-age orogenic highlands (hereafter CAMOH) and the areal extent of the CAMOH are less well-constrained. Nevertheless, it is crucial to obtain such information because of the influence that the elevation of this orogen may have had on the climatic, tectonic, and landscape evolution of the North American Cordillera.

At a global or hemispheric scale, increased elevation can result in changes in the planetary wave pattern or albedo and significant reorganizations of climate (e.g. Broccoli and Manabe, 1992; Ruddiman and Kutzbach, 1989). At local and regional scales, increased elevation results in surface cooling as a result of the adiabatic lapse rate and changes in net moisture balance as a result of disrupted atmospheric circulation and/or the development of rain shadows and enhanced orographic precipitation (e.g. Drummond et al., 1996; Ehlers and Poulsen, 2009; Fricke et al., 2010; Poulsen et al., 2010; Zaleha, 2006) as well as a host of other, resultant feedbacks (e.g. increased albedo of higher, colder, dryer, less-vegetated surfaces). In turn, climatic conditions may influence rates of uplift and rock exhumation (e.g. Reiners et al. 2003; Wobus et al., 2003) and foreland basin subsidence and infilling (e.g. Zaleha, 2006).

A number of different methods have been developed to study the paleoelevation of ancient mountain belts (e.g. rock mechanics: DeCelles and Coogan, 2006; leaf physiognomy: Gregory and Chase, 1992; Wolfe et al., 1998; stable isotope paleoaltimetry: Chamberlain

* Corresponding author. Tel.: +1 484 646 5864; fax: +1 610 683 1352.
E-mail address: sewall@kutztown.edu (J.O. Sewall).

0012-821X/$ - see front matter © 2012 Elsevier B.V. All rights reserved.
http://dx.doi.org/10.1016/j.epsl.2012.12.002

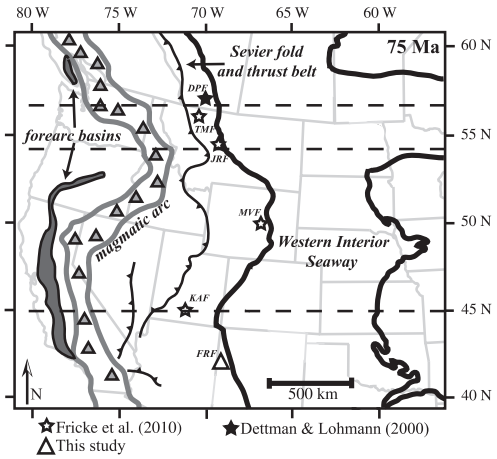

Fig. 1. Campanian paleogeographic map of western North America (after Fricke et al., 2010) showing sample locations (stars and triangles; DPF=Dinosaur Park Formation; TMF=Two Medicine Formation; JRF=Judith River Formation; MVF=Mesa Verde Formation; KAF=Kaiparowits Formation; FRF=Fossil Forest member of the Fruitland Formation), analytical transect locations (horizontal dashed lines), highland locations, and interior seaway extent.

et al., 1999; Crowley et al., 2008; Garzione et al., 2000; Mulch et al., 2006; Rowley et al., 2001), and some of the most promising rely on changes in the oxygen isotope ratios of precipitation, which can correlate with changes in elevation. The primary reason for such a correlation is the preferential incorporation of ^{18}O into condensate as water is precipitated and removed from cooling air masses. As more precipitation is removed from an air mass, the oxygen isotope ratio ($\delta^{18}O$) of the remaining vapor becomes progressively lower. Resulting patterns in $\delta^{18}O$ of precipitation ($\delta^{18}O_{pt}$) include a regular decrease in $\delta^{18}O_{pt}$ as air masses cool while rising over mountains (e.g. Dansgaard, 1964; Gat, 1996; Rozanski et al., 1993), thus, changing patterns in $\delta^{18}O_{pt}$ can reflect changes in local elevation. The combination of this relationship with observed isotopic lapse rates and/or Rayleigh distillation models has allowed researchers to estimate the paleoelevation of significant topographic features (e.g. Bissig and Riquelme, 2010; Garzione et al., 2008; Hren et al., 2010; Kent-Corson et al., 2009, 2006; Kohn et al., 2002; Poage and Chamberlain, 2002, 2001; Rowley et al., 2001). However, it should be noted that, while the association with increasing elevation is a robust one, regular decreases in $\delta^{18}O_{pt}$ can also be associated with other climatically or tectonically influenced factors such as changes in original moisture source, increasing distance from moisture source, increased length of meridional transport paths, mixing of air masses with different transport histories, and non-adiabatic cooling (e.g. Dansgaard, 1964; Ehlers and Poulsen, 2009; Gat, 1996; Poulsen et al., 2010; Rozanski et al., 1993), all of which can pose difficulties to accurately estimating paleoelevation from $\delta^{18}O_{pt}$ (e.g. Ehlers and Poulsen, 2009). Due to this potential for complex or confounding interactions and feedbacks between changing tectonics and climate (e.g. Galewsky, 2009; Molnar and England, 1990; Ruddiman and Kutzbach, 1990), many researchers have employed increasingly holistic, nuanced approaches to paleoelevation estimation (e.g. consideration of basin hydrology: Davis et al., 2008, 2009; Hough et al., 2011; quantification/consideration of interactions between tectonics and climate: Ehlers and Poulsen, 2009; Kent-Corson et al., 2009; consideration of climate change: Hren et al., 2010; Molnar, 2010).

Given recent advances in general circulation models (e.g. Mathieu et al., 2002; Noone and Sturm, 2010; Zhou et al., 2008), one of the most straightforward methods for integrating the complex feedbacks between climate, tectonics, and the isotopic signature of precipitation is to simulate past climates with an atmospheric general circulation model (AGCM) enabled with the ability to trace the various species of water isotopes (i.e. ^{16}O, ^{17}O, ^{18}O, ^{1}H, ^{2}H). Variation of the topographic boundary conditions in such simulations (e.g. Poulsen et al., 2010) and comparison between simulated isotopic values in meteoric waters and those derived from oxygen-bearing minerals precipitated or secreted in equilibrium with terrestrial surface waters can offer insight into the development of ancient orogenic features. Here we integrate isotope-tracer-enabled AGCM simulations of Campanian climate and $\delta^{18}O$ data derived from unionid bivalves and soil carbonates to investigate the paleoelevation of the CAMOH of western North America.

2. Modeling methods

We used the National Center for Atmospheric Research (NCAR) Community Atmosphere Model v. 3 (CAM3; Collins et al., 2006) with an integrated isotope tracer code (isoCAM3; Noone, 2003; Noone and Sturm, 2010) to conduct five, fixed lower boundary condition, atmosphere-only simulations of Campanian climate with varying mean elevations for the CAMOH (Table 1). isoCAM3 utilizes a third-generation isotope tracer scheme (Noone and Sturm, 2010) and is coupled to a dynamic land surface model (CLM3: Bonan et al., 2002; Oleson et al., 2004) where the isotopic composition of terrestrial water and evapotranspiration are accounted for by a simple two-bucket scheme (Noone and Simmonds, 2002). Present-day simulations with isoCAM3 have been validated against the Global Network of Isotopes in Precipitation (GNIP; IAEA/WMO, 2006) and show good agreement with observed isotopic patterns at both global and regional scales (Noone, 2003; Speelman et al., 2010).

For all five of our Campanian model simulations, global topography, geography, and vegetation were modified from previously published Cretaceous boundary conditions (Otto-Bliesner et al., 2002; Sewall et al., 2007; see Fricke et al., 2010 for global maps). A monthly varying seasonal cycle of sea surface temperatures (SST) was developed from an equilibrated, fully coupled Campanian simulation of the NCAR Climate System Model (CSM v. 1.4) (Otto-Bliesner et al., 2002). Global land surface conditions and sea surface temperatures are invariant across our five simulations (Table 1). Atmospheric composition was also held constant with pCO_2 specified at 1680 ppm, pCH_4 at 700 ppb, and pN_2O at 275 ppb (Table 1); these are similar to the greenhouse gas concentrations associated with our SST distribution (Otto-Bliesner et al., 2002). Orbital parameters in all cases were

Table 1
Boundary conditions for Campanian climate simulations.

Simulation parameter	Value (s)
Invariant parameters	
pCO_2	1680 ppm
pCH_4	700 ppb
pN_2O	275 ppb
Orbital configuration	Modern
Vegetation distribution	Fricke et al. (2010)
Global topography/geography	Fricke et al. (2010)
Solar constant	1355 W/m^2
Sea surface temperature distribution	Fricke et al. (2010)
$\delta^{18}O$ value of global ocean	−1‰
Variable parameters	
Average elevation of the CAMOH	1200 m
	2000 m
	2800 m
	3500 m
	3975 m

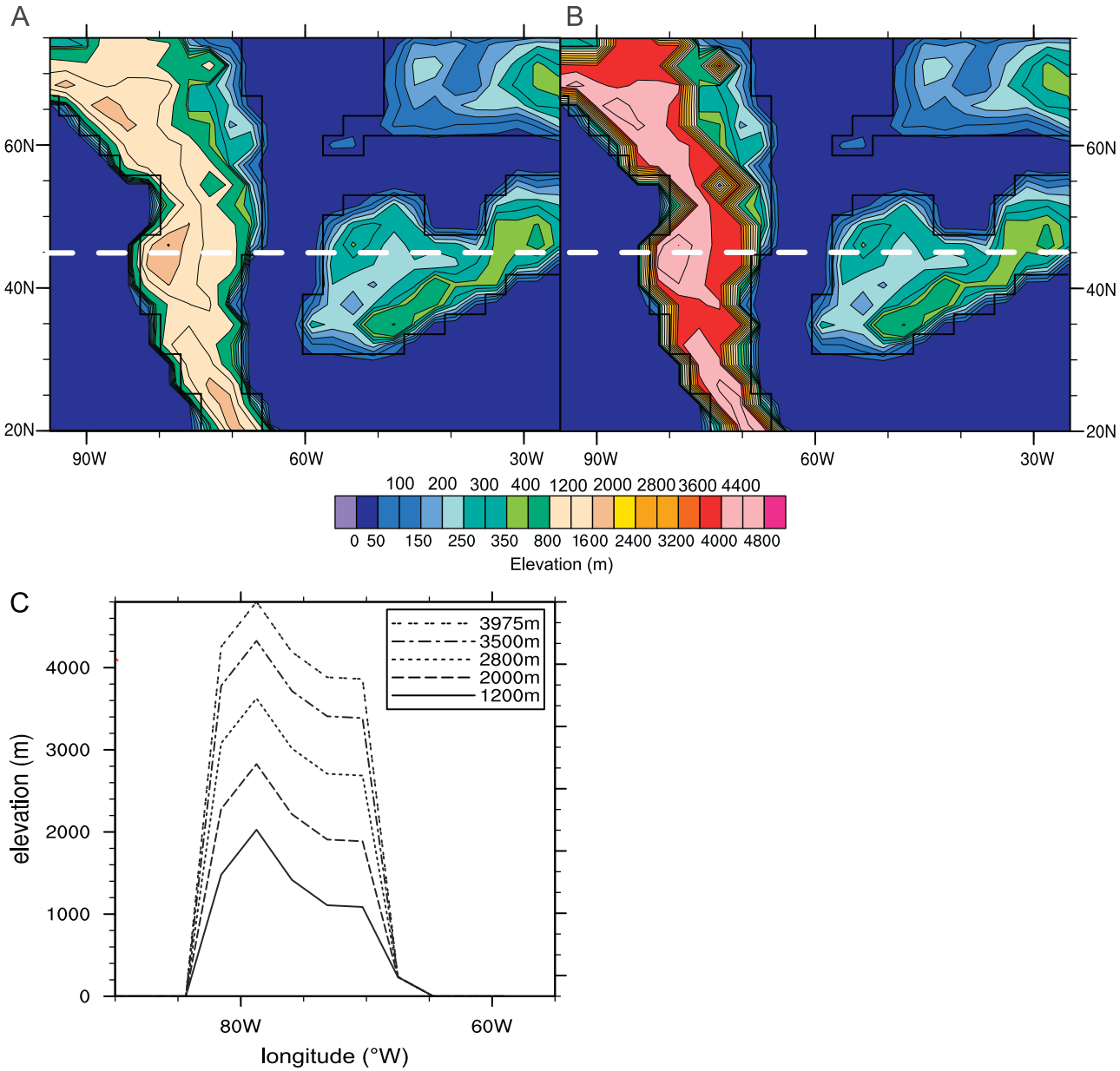

Fig. 2. Western North American elevation boundary conditions for Campanian climate simulations. (A) Minimum topography with a CAMOH average of 1200 m. (B) Maximum topography with a CAMOH average of 3975 m. (C) An example zonal transect across 45°N (heavy dashed line in panels (A) and (B) showing local variation through all average elevations (1200–3975 m); elevations outside of the Cordillera or below 500 m were unchanged between simulations.

specified at modern values and the solar constant was reduced to 1355 W/m^2 (Table 1). isoCAM3 was set up to simulate the H_2O and $H_2{}^{18}O$ content in both precipitation and water vapor with a fixed, ice-free global ocean value of −1‰ $\delta^{18}O$ for all simulations (Table 1). All simulations were conducted with 26 vertical levels in the atmosphere and a horizontal resolution of spectral T42 (~2.8° latitude × 2.8° longitude).

The model parameter that was allowed to vary across our five simulations was the average elevation of the CAMOH between northern Mexico and western Alaska (Table 1). The base topographic conditions of Fricke et al. (2010; average CAMOH elevation of 2000 m) were uniformly increased or decreased over western North America to achieve average CAMOH elevations that ranged from 1200 m to 3975 m (Fig. 2; Table 1). While the average elevation of the CAMOH varied, the topographic roughness and lowest elevations (areas below 500 m elevation, predominantly those proximal to coastlines) were invariant, so the locations of local peaks (higher than the average elevation) and valleys (lower than the average elevation) were constant across the simulations (Fig. 2C). Each of the five simulations with increasing CAMOH elevation was integrated for 30 model years with the final 10 years of the equilibrated simulation averaged for paleoclimatic analyses. Simulated $\delta^{18}O$ of precipitation was then weighted according to the volume of precipitation falling in an area over time and simulated isotopic values were compared to proxy records of $\delta^{18}O$ of surface water (Table 2).

3. Results

Although the simulations conducted in this work were global, only results from western North America will be presented and

Table 2
Proxy-derived estimates of Campanian surface water $\delta^{18}O$ (VSMOW scale) in Western North America (after Fricke et al., 2010).

Formation[a]	Depositional environment	Sample size	Mean (‰)	Median (‰)	Range (max/min) (‰)
DPF[b,c]	Large river	128	-17.2 ± 2.8	-17.0	$-14.8/-21.3$
TMF[b]	Stream	7	-8.6 ± 1.5	-8.8	$-7.6/-9.7$
TMF[b]	Soil (at 24 °C)	13	-8.2 ± 1.1	-8.1	$-7.0/-9.1$
JRF[b]	Pond	6	-7.6 ± 1.0	-7.4	$-7.2/-8.3$
JRF[b]	Large river	19	-16.2 ± 2.8	-16.2	$-13.5/-18.7$
MVF[b]	Stream	3	-14.7 ± 1.5	-14.7	$-14.0/-15.5$
KAF[b]	Pond	6	-8.2 ± 0.9	-8.0	$-7.8/-8.9$
KAF[b]	Large river	8	-16.2 ± 0.5	-16.2	$-16.0/-16.7$
FRF[d]	Stream	11	-7.6 ± 1.7	-7.6	$-4.5/-9.8$

[a] See Fig. 1 for formation abbreviations.
[b] Information presented in Fricke et al. (2010).
[c] Includes bivalve data originally presented in Dettman and Lohmann (2000).
[d] Bulk samples of unionid bivalves. $\delta^{18}O$ of surface water calculated as in Fricke et al. (2010).

discussed here (see inset boxes in Figs. 3A and 4). Furthermore, as the study region exhibited pronounced precipitation seasonality in all simulations, we present not only annual averaged results, but also wet and dry season averages. The wet season is defined as all individual months during which $>8\%$ of the annual precipitation falls and is associated with generally onshore atmospheric flow of water-laden air masses from the interior seaway toward the foreland (Fig. 3). The dry season, associated with generally offshore atmospheric flow, constitutes the remainder of the year. With increasing CAMOH elevation, the duration and intensity of this seasonally reversing (i.e. monsoonal) circulation increased while the time of the year at which the seasonal reversal took place gradually became later (Fig. 3).

In addition to affecting the duration, intensity, and timing of the regional monsoon, increasing highland elevation caused temperatures over the highlands to fall from $\sim$22 to $\sim$15 °C during the wet season and from $\sim$15 to $\sim$0 °C during the dry season (Fig. 3). Coastal plain temperatures, however, change only slightly from $\sim$22 to $\sim$27 °C as highland elevations increase (Fig. 3). Rising highlands also lead to an increase in precipitation, particularly during the wet season, with amounts along the eastern CAMOH front increasing from as little as 60 cm to over 400 cm (Fig. 3) over the entire foreland basin.

Annual average simulated $\delta^{18}O$ values (VSMOW) for precipitation are presented in map view in Fig. 4 and as latitudinal transects in Fig. 5. As highland elevation increases, $\delta^{18}O$ of precipitation falling in or feeding into highland areas of the study region becomes lighter, moving from ~ -8‰ (Figs. 4A; 5; Table 3) to as low as -18‰ (Figs. 4E; 5; Table 3). $\delta^{18}O$ of precipitation in coastal regions <500 m in elevation is ~ -7.5‰ and only varies $\pm \sim 1$‰ in response to changes in highland elevations (Figs. 4 and 5; Table 3). Similar elevation-related changes in $\delta^{18}O$ of precipitation are simulated for wet and dry seasons, with $\delta^{18}O$ values during the wet season being more positive than the annual average, and $\delta^{18}O$ of precipitation during the dry season being somewhat more negative (Table 3).

4. Discussion

Modeled $\delta^{18}O$ of precipitation varies over a wide region in response to increasing mean elevation of the CAMOH. Integrating these variations with an isotopic record of Late Cretaceous precipitation from the study area allows us to investigate the paleotopography of the CAMOH. Proxy records of $\delta^{18}O$ of surface water are available for a number of Campanian foreland basin localities that span paleolatitudes from 42–57°N (Fig. 1), but the focus of our analysis is on three latitudinal transects (45, 54 and 56.5°N) where the most oxygen isotope data are available. At each locality, bulk samples of unionid bivalves and soil carbonates were taken, and estimates of $\delta^{18}O$ of associated surface waters were made (Dettman and Lohmann, 2000; Fricke et al., 2010). Paleosol nodules and bivalves from ponds and small streams produce estimates of surface water $\delta^{18}O$ with mean values of ~ -8‰ (Table 2; Fig. 5), and these waters are interpreted to represent small, coastal plain catchments that were recharged by local precipitation from air masses that had not traveled far from the moisture source (the interior seaway). In contrast, bivalves found in large river deposits cluster at a much lower mean value of ~ -17‰ (Table 2; Fig. 5), indicating a larger degree of isotopic rainout and suggesting that high elevation catchments were the dominant source of recharge for major river systems crossing the foreland basin (e.g. Fricke et al., 2010). The relatively constant offset of $\sim$9‰ between the estimated $\delta^{18}O$ of coastal plain surface waters and those from higher elevations is compared to simulated values to provide constraints on the elevation and extent of the CAMOH.

4.1. Model-data comparisons and paleoelevation

As noted above, we focus our analysis on three latitudinal transects that cover the area where carbonate data were obtained. We also focus on annual $\delta^{18}O_{pt}$ simulated by the model because of the strong relationship between the mean $\delta^{18}O$ of fluvial waters and $\delta^{18}O$ from bulk samples of unionid bivalve shells (Kohn and Dettman, 2007).

Along the coastal plain (<500 m, $\sim$67°W), where orography is constant and wet season air masses move primarily from east to west in all simulations (Fig. 3), modeled $\delta^{18}O_{pt}$ is relatively invariant regardless of latitude or elevation of the adjacent highlands and matches $\delta^{18}O$ of surface waters inferred from bivalves and soil carbonates relatively well (Table 3; Fig. 5). Modeled $\delta^{18}O_{pt}$ values for high elevation precipitation, however, decrease steadily with increasing highland elevation. The magnitude of this decrease is not regionally constant, with greater decreases in $\delta^{18}O$ of precipitation occurring along transects with the highest average elevation (Fig. 5). This pattern emphasizes the role of elevation in cooling air masses, initiating precipitation (precipitation [total, large-scale, and convective] increases linearly [$r^2=0.97$] with increasing elevation [not shown]), and progressively removing ^{18}O from the atmosphere. Although we do find the greatest changes in $\delta^{18}O_{pt}$ when CAMOH elevations reach ± 2000m (Fig. 5) and find that the particular elevation gain that engenders the greatest change in $\delta^{18}O_{pt}$ varies meridionally along the mountain belt (e.g. Fig. 5A and C), our results suggest a more uniform decrease in $\delta^{18}O_{pt}$ with increasing elevation than that observed in similar modeling studies of the Andes Mountains (Insel et al., 2012; Poulsen et al., 2010). The different patterns simulated in these two regions could reflect real differences in how climate, $\delta^{18}O_{pt}$, and topography relate in these two different situations. For example, the progressive increases in precipitation and consequent reduction in $\delta^{18}O_{pt}$ that we simulate may indicate stable atmospheric conditions where only forced lifting and cooling of air masses at the local lapse rate contributes to increased precipitation. Given the approximately linear tropospheric lapse rate, this would result in a linear precipitation response. Conversely, thresholded behavior in Andean simulations (Insel et al., 2012; Poulsen et al., 2010) could reflect more unstable atmospheric conditions where imposed elevation increases can force air parcels above the level of free convection and drive sudden, non-linear increases in precipitation that do

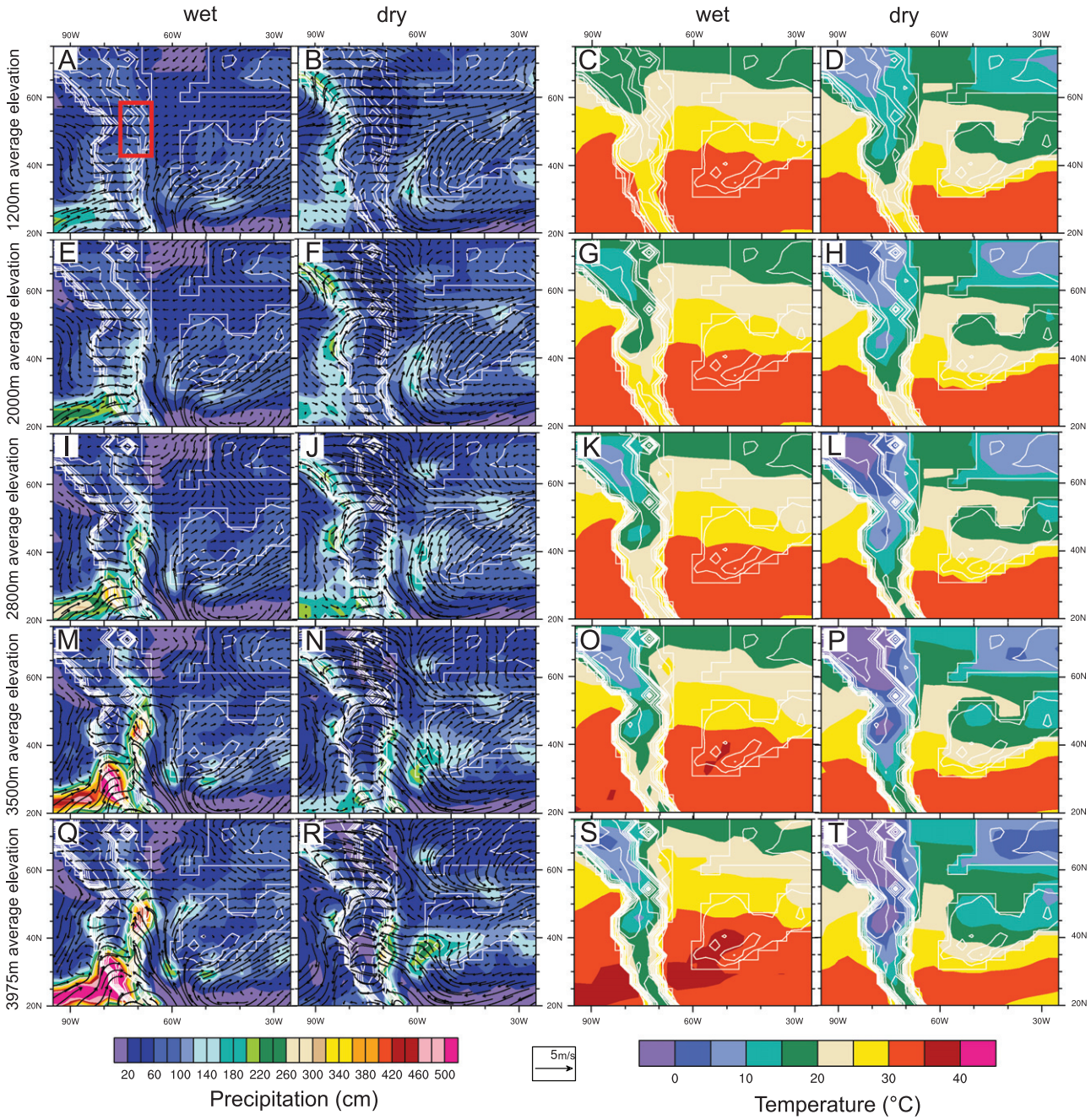

Fig. 3. Simulated Campanian climate of North America with increasing CAMOH elevation (white contour lines in all panels). The study area from which data were collected is outlined in red in panel A. Panels A–D have a 1200 m average highland elevation, E–H have a 2000 m average highland elevation, I–L have a 2800 m average highland elevation, M–P have a 3500 m average highland elevation, and Q–T have a 3975 m average highland elevation. Stronger onshore flow and enhanced precipitation differentiate the WET season (April through August for 1200–2800 m average highland elevation; April–September for 3500 m average highland elevation; May–October for 3975 m average highland elevation; Panels A, C, E, G, I, K, M, O, Q, S) from the DRY season (Panels B, D, F, H, J, L, N, P, R, T). Panels A, B, E, F, I, J, M, N, Q, and R show overall increasing precipitation (color map) and more pronounced meridional and onshore (over the coastal plain in the foreland basin) surface flow (vector field) with increasing highland elevation in all seasons. Both precipitation and East–Southeasterly surface flow are stronger with increasing elevation in the WET season (Panels A, E, I, M, Q) than in the DRY season (Panels B, F, J, N, R). Panels C, D, G, H, K, L, O, P, S, and T show high elevation and DRY season cooling (color map) across North America as CAMOH elevation increases. WET season temperatures east of the highlands, however, warm with increasing elevation (Panels C, G, K, O, S), increased precipitation, and strengthening South-Southeasterly surface flow (Panels A, E, I, M, Q).

not continue to grow as rapidly with further elevation increases (Poulsen et al., 2010). Alternatively, the different patterns could reflect artifacts of how modeling was undertaken in each study (e.g. lowest elevation considered, number of elevation 'steps' that were simulated). Additional model simulations are needed to investigate these possibilities and they are ongoing.

In this study, simulations where mean elevations are less than 2800 m generally have modeled $\delta^{18}O$ of highland precipitation that is higher than those surface water values indicated by bivalve data (Table 3; Fig. 5). It is only at average CAMOH elevations of 3500–4000 m that $\delta^{18}O_{pt}$ values for the highest elevation recharge agree with those measured from large-river-dwelling

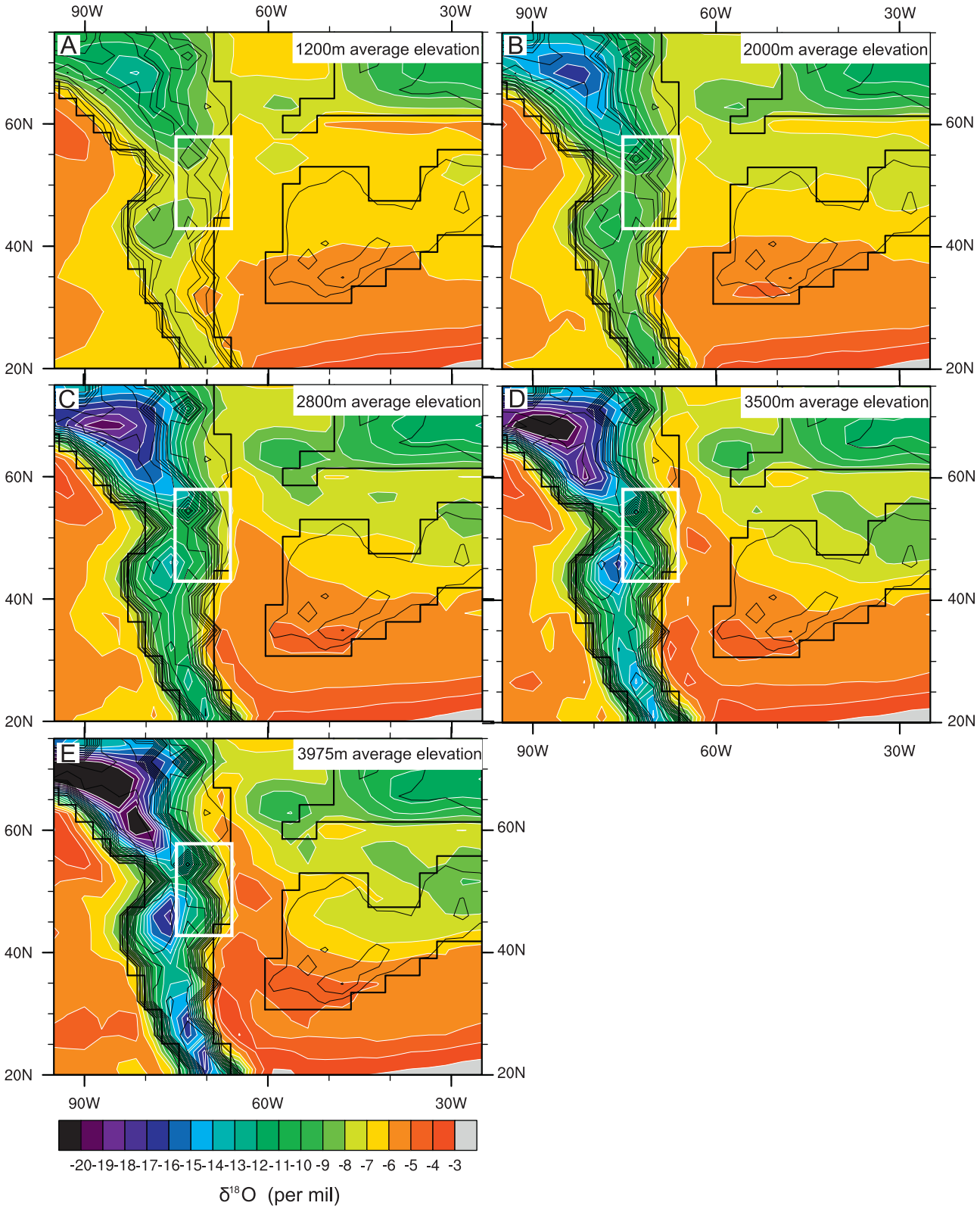

Fig. 4. Annual average, precipitation-volume weighted, $\delta^{18}O$ values (VSMOW; color map, white contours) in simulated Campanian precipitation with increasing CAMOH elevation (black contour lines; contour interval = 200 m from 0–1000 m and 400 m from 1000–4200 m). Increasing average highland elevation from 1200 m (A) to 3975 m (E) results in more negative $\delta^{18}O$ values in precipitation over the highlands and eastern North America, while values over the interior seaway/foreland grow increasingly positive with increasing elevation (this increase in foreland $\delta^{18}O$ values is consistent with both observed data (e.g. Mulch et al., 2010) and simulations (Jeffrey et al., 2012) of the Andean foreland). Simulated $\delta^{18}O$ values in precipitation over the study region (white boxes in figure) coastal plain are generally invariant or become slightly more positive with increasing elevation. Simulated $\delta^{18}O$ values in precipitation over the highlands and in the extended catchment (west of the white box to the continental divide) become increasingly negative with increasing elevation. (For interpretation of the references to color in this figure legend, the reader is referred to the web version of this article.)

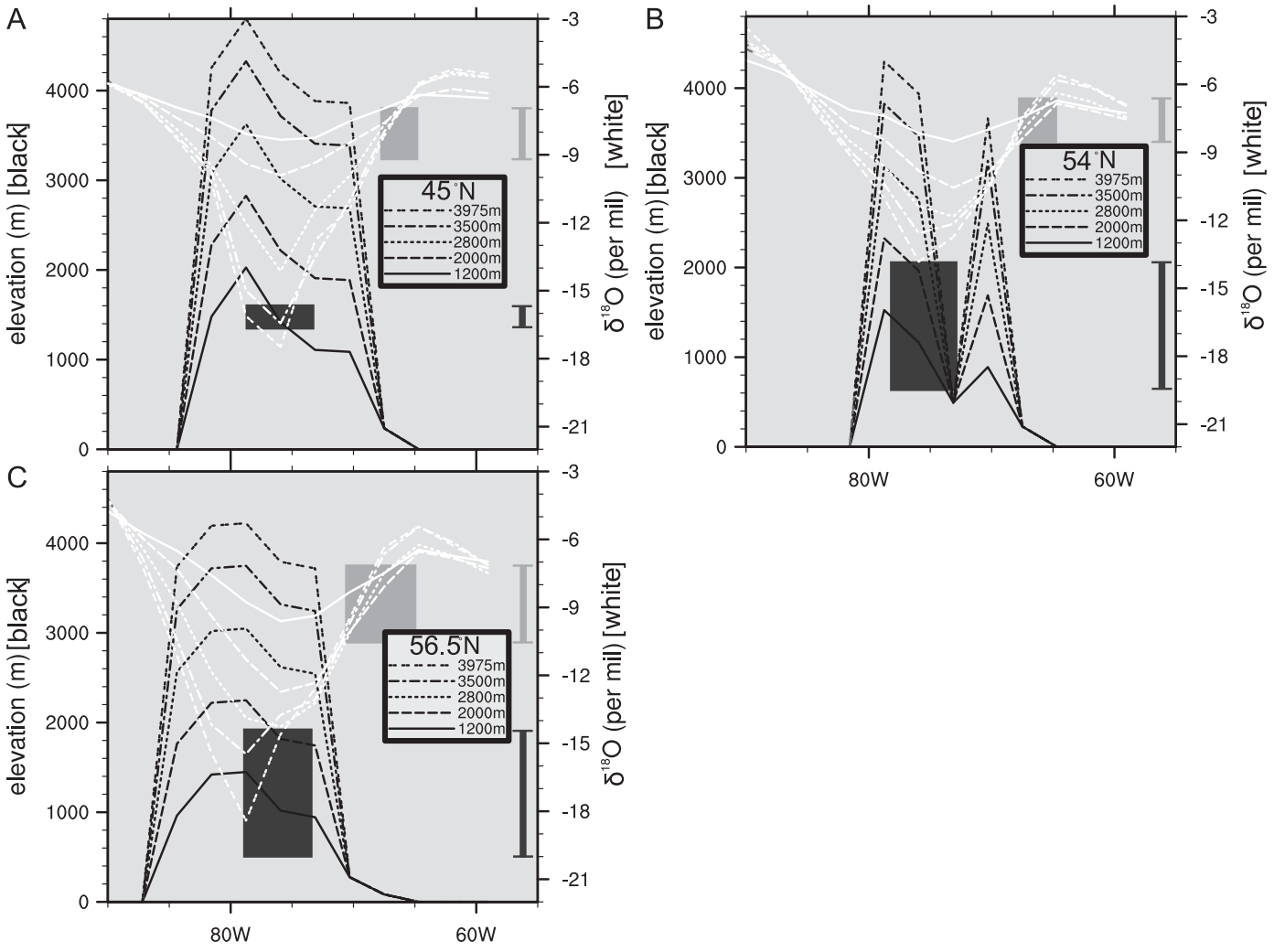

Fig. 5. Annual average, precipitation-volume weighted, $\delta^{18}O$ values (VSMOW; white lines) in simulated Campanian precipitation with increasing CAMOH elevation (black lines) for three zonal transects across the highlands. Transect latitudes correspond to those latitudes where bivalve and soil carbonate data were collected (see Fig. 1; Note: The invariant valley depth at ~73°W in panel B is an artifact of the topographic perturbation method (see Section 2) and the resulting "double-peaked" topography in this location likely biases local $\delta^{18}O_{pt}$ to somewhat more positive values than the broader, elevated plateaux in the other transects.). Simulated $\delta^{18}O$ values in precipitation over the coastal plain are generally invariant or become slightly enriched with increasing elevation and all correspond well to measured $\delta^{18}O$ values (light grey bars and box heights show mean measured value $\pm 2\sigma$. Light grey box widths highlight the location of the modeled coastal plain). Simulated $\delta^{18}O$ values in precipitation over the highlands become increasingly depleted with increasing elevation and only those values corresponding to average highland elevations of 3500 or 3975 m correspond well to measured $\delta^{18}O$ values (dark grey bars and box heights show mean measured value $\pm 2\sigma$. Dark grey box widths highlight the location of the modeled highland recharge area).

bivalves (Table 3; Fig. 5); the best match is achieved when the average elevation of the CAMOH approaches 4000 m.

4.2. Advantages of an integrated model-data approach for reconstructing paleoelevation

Our paleoelevation estimate of ~3500–4000 m for the CAMOH is generally similar to that obtained from the simple application of the most commonly applied isotope paleoaltimeter (the global average isotopic lapse rate [2.8‰ km^{-1}]; Poage and Chamberlain, 2001) to the 9‰ isotopic offset that we identify in the proxy data. Using this approach, a 9‰ offset and a 2.8‰ km^{-1} lapse rate indicate paleoelevation of 3214 m for the CAMOH. The similarity between this value and our estimate may call into question the need for the model-data technique that we describe here. However, a detailed consideration of *why* this similarity exists serves to illustrate the limitations associated with the simple application of lapse rates while highlighting the corresponding utility of our model-data approach.

Application of average isotopic lapse rates to determine paleoelevation relies on the assumption that regional moisture sources, transport paths, and their relative contributions are well known. This implies *a priori* knowledge of ancient, regionally specific atmospheric dynamics. This information is, in fact, not often well known; using an isotope-tracer-enabled AGCM provides us with the framework of a single, major moisture source for the eastern front of the CAMOH (the WIS), highly seasonal precipitation delivery in the warmer months of the year, and moisture paths from source to sink that are relatively short and straight (Fig. 3). In this relatively simple climatic situation, a lapse rate calculation provides a reasonable paleoelevation value; this is unlikely to be true in more complex environments. Our approach, which integrates climate simulations and isotopic data, provides confidence that the potential complexities of regional climate and/or tectonic factors have been considered (e.g. changes in original moisture source, increasing distance from moisture source, increased length of meridional transport paths, mixing of air masses with different transport histories, and non-adiabatic

Table 3
Simulated $\delta^{18}O_{pt}$ for the CAMOH front.

Mean highland elevation (m)	Latitude (°N)	Annual average $\delta^{18}O$ (‰)		Wet season [a] average $\delta^{18}O$ (‰)		Dry season average [b] $\delta^{18}O$ (‰)	
		High peaks value	Coastal plain value	High peaks value	Coastal plain value	High peaks value	Coastal plain value
1200	45	−8.3	**−7.0**	−7.5	−6.7	−9.8	−7.7
	54	−8.5	**−7.5**	−7.8	−7.3	−9.6	−7.9
	56.5	−9.6	**−7.5**	−8.7	−7.4	−10.7	−7.7
2000	45	−9.9	**−7.6**	−8.5	−7.3	−11.7	−8.3
	54	−10.6	**−8.4**	−9.4	−8.2	−14.6	−8.7
	56.5	−12.7	**−8.1**	−11.2	−7.6	−15.4	−9.1
2800	45	**−14.1**	**−7.7**	−11.2	−7.3	−16.1	−8.2
	54	−11.8	**−8.0**	−10.0	−7.7	−12.4	−8.9
	56.5	**−14.3**	**−7.5**	−11.8	−6.7	−18.0	−8.8
3500	45	**−16.4**	**−8.0**	−12.7	−7.3	−19.4	−8.8
	54	−12.6	**−7.6**	−10.3	−7.4	−15.3	−8.1
	56.5	**−15.5**	**−6.6**	−12.2	−5.9	−19.2	−7.8
3975	45	**−17.5**	**−8.2**	−14.0	−7.1	−20.6	−9.1
	54	**−13.8**	**−7.5**	−11.8	−7.4	−15.5	−7.6
	56.5	**−18.4**	**−6.4**	−14.3	−5.7	−20.2	−7.2

Note: Bold values in the annual average column indicate match between simulated $\delta^{18}O$ values in precipitation and those measured from bivalves and soil carbonates (see also Fig. 5).

[a] April through August for 1200–2800 m average highland elevation; April–September for 3500 m average highland elevation; May–October for 3975 m average highland elevation.

[b] All months not included in the wet season.

cooling; Dansgaard, 1964; Ehlers and Poulsen, 2009; Gat, 1996; Poulsen et al., 2010; Rozanski et al., 1993) and, consequently, provides a more robust paleoelevation estimate than simple application of an isotopic lapse rate calculation.

Furthermore, application of the modern global-average isotopic lapse rate assumes that the modern lapse rate can be applied to the past. This is not necessarily true. Isotopic lapse rates are not consistent through earth history but rather vary through time with warmer intervals having shallower vertical lapse rates (Poulsen and Jeffery, 2011). Application of modern isotopic lapse rates in warm paleoclimates may, therefore, lead to underestimation of paleoelevation, and the use of isotope-tracer-enabled GCMs has been suggested to address this source of error (Poulsen and Jeffery, 2011). By providing an internally consistent realization of Campanian climate, our simulations suggest that the vertical isotopic lapse rate for $\delta^{18}O$ in this region was more accurately 2.26‰ km^{-1} rather than the modern value of 2.8‰ km^{-1} (Poage and Chamberlain, 2001); simple application of the modern value (as shown above) underestimates our best-fit elevation by ~20%. The use of an isotope-tracer-enabled AGCM thus provides a better result.

Finally, and perhaps most fundamentally, in contrast to the more one-dimensional, "points on a map" elevation estimates produced by traditional, isotopic lapse-rate-based paleoelevation techniques, our approach interprets paleoelevation in terms of a geographically extensive region with a prescribed topographic roughness and average elevation. Many studies of the tectonic mechanisms that drive landscape evolution and climate change are generally regional in nature. Treating paleoelevation in this fashion provides the broad perspective and frame of reference that those investigations require.

4.3. Characterizing paleoelevation at the regional scale

Although our approach has the advantage of integrating climate and isotopes to quantify topographic features over large spatial scales, unknowns and assumptions inherent in the various disciplines that we integrate (Table 4) both contribute to some uncertainty in our paleoelevation estimates and limit our ability to provide high-resolution bounds on the specifics of an ancient orogen (i.e. we cannot predict exact elevation, nor provide a standard error in elevation, for a specific location). There is, however, no reasonable or likely combination of those unknowns that can substantially alter the isotopic offset between highland and lowland areas that is inferred from proxy data (Table 4), and, given the general agreement between our simulated climate and proxy climate indicators (Table 4), we are confident that, while details of the topography remain obscure, the CAMOH were a significant topographic feature with high elevations on the order of at least 3500–4000 m.

Because our integrated model-data approach has the benefit of being able to quantify the basic paleoelevational characteristics of a broad region (e.g. mean elevation and lateral extent) but is limited in resolving local details (e.g. accurate relief at kilometer scales), we suggest that it may be most parsimonious to treat the topographical study of ancient orogens akin to the sedimentological study of ancient depositional environments. The goal of the latter is not an exhaustive description of all details of that environment such as water flow rate, water depth etc., but to infer the presence of a general type of environment using a prescribed set of diagnostic characteristics such as sediment size, shape, sorting, etc. preserved in the rock record that can be interpreted using modern analogs. For orogens studied with the aid of climate models, the impact of specified paleotopography on the spatial pattern of $\delta^{18}O_{pt}$ should be sufficient to quantify the overall topographic characteristics (average elevation, width, and length) of the orogen and, thus, permit the identification of quantitatively analogous modern landforms.

In the case of this study, Late Cretaceous orogenic highlands with a length of ~3000 km, width of ~300 km and a mean elevation approaching 4000 m produce a good match between model and proxy data. These topographic characteristics are similar to those of the Andes Mountains in South America, and, thus, we can conclude that the CAMOH must have been of "Andean-scale" in their basic topographic characteristics.

5. Conclusions

In this study we address the inherent complexity of the interactions between climate, tectonics, and oxygen isotopic values (e.g. Ehlers and Poulsen, 2009; Galewsky, 2009; Molnar and England, 1990; Molnar, 2010) by using measured and simulated $\delta^{18}O$ precipitation values to estimate the paleoelevation of the CAMOH in western North America. Oxygen isotopic offset between local coastal plain and remote high elevation recharge measured in soil carbonates and freshwater bivalves suggests significant relief existed across the CAMOH front. Comparison of modeled and measured precipitation $\delta^{18}O$ values indicates that the average elevation of the CAMOH must have exceeded 3000 m and that mean highland extent was very likely on the order of the modern Andes Mountains. By describing paleoelevation as a three dimensional topographic feature, we provide a model for the highlands that, while open to refinement,

Table 4
Sources of uncertainty in paleotopographic quantification.

Source of uncertainty	Potential impact on paleotopographic quantification
Prescribed $\delta^{18}O$ of the interior seaway	Changes in seaway $\delta^{18}O$ would impact absolute simulated values for $\delta^{18}O_{pt}$ but not the offset between highlands and lowlands. Furthermore, geochemical constraints (e.g. Fisher and Arthur, 2002; Cochran et al., 2003; He et al., 2005) suggest that the $\delta^{18}O$ of the seaway could be no more than 2.5‰ lower than our prescribed value, and decreases greater than this would result in no agreement between simulated and measured $\delta^{18}O$ values for coastal plain ponds, soils, and streams.
Averaging of upstream precipitation signatures in bulk fluvial $\delta^{18}O$ values	Averaging of lighter high elevation precipitation and heavier low elevation precipitation would make bulk fluvial $\delta^{18}O$ higher than the highest elevation precipitation and, thus, result in underestimates of paleoelevation.
Precise temperature and seasonal timing of soil carbonate and bivalve shell formation is unknown	If bivalve shell values represent seasonal precipitation rather than annual average, elevation estimates could be either slightly lower (dry season bias) or higher (wet season bias). Given that the wet season comprises 60–70% of regional precipitation, a wet season bias seems more likely. If bivalve shells formed at temperatures other than the specified optimal temperature of 21 °C (Kohn and Dettman, 2007), then elevation estimates could also be either lower (formation at warmer temperatures) or higher (formation at cooler temperatures). Given the available information on bivalve growth with respect to water temperature (Kohn and Dettman, 2007), it is difficult to identify which of these biases, if either, might be at play in this study. Finally, if soil carbonates formed at modeled soil temperatures (27 °C—not shown) rather than the assumed 24 °C temperature (Table 1), the $\delta^{18}O$ values presented in Table 1 would decrease by 0.9‰; the resulting values (~ -8 to -10‰) would still be in line with the other measured coastal plain values and, therefore, have little impact on our paleoelevation estimates.
Model spatial resolution is coarser than that of proxy data and proxy data spatial coverage is limited compared to model results	The scale mismatch between model and proxy data makes direct, local comparisons difficult. However, changes in such local details are unlikely to influence the regional climate signal that requires ± 3975 m CAMOH to produce an annual average highland/lowland offset in $\delta^{18}O_{pt}$ of $\sim$9‰.
Simulated Campanian climate	It has recently been shown that under different climate regimes, the vertical lapse rate of $\delta^{18}O_v$ changes, with warmer climates having shallower vertical lapse rates (Poulsen and Jeffery, 2011). Simulated climates that are too warm or too cold will, thus, result in incorrect isotopic gradients in the model and paleoelevation estimates that are too high or low, respectively. Comparison of our simulated climate to proxy climate indicators suggests that our simulation produces the Campanian climate of western North America reasonably well. Sedimentological and isotopic evidence indicate a warm, wet climate with seasonal aridity or episodic precipitation (Roberts, 2007; Straight et al., 2004) similar to that in our simulations (Fig. 3A, B, E, F, I, J, M, N, Q, R). Our modeled mean annual temperatures (MAT) of 17–27 °C in the coastal plain of the study region (not shown) agree well with both faunal (Markwick, 1998) and floral (Saward, 1992; Vakhrameev, 1991; Wolfe and Upchurch, 1987) estimates that suggest Campanian MAT in this region exceeded $\sim$15 °C. Cold (dry) season temperatures of 5–20 °C (Fig. 3D, H, L, P, T) agree well with faunal indicators of cold month mean temperatures (CMM) > 5.5 °C (Markwick, 1998). Warm (wet) season temperatures of 15–30 °C (Fig. 3C, G, K, O, S) are, however, somewhat cooler than recent clumped isotope estimates of 30–40 °C just east of the Sevier front (Snell, 2011), although the latter may be overestimates (Snell et al., in press). Given that the largest discrepancy between our simulated climate and the available proxy data is a somewhat cool bias in the warm (wet) season (Snell, 2011), our paleoelevation estimate for the CAMOH could be low. However, general agreement between modeled and proxy-derived MAT and CMM suggests that any elevation underestimate resulting from a climate bias in our simulations is likely small.
Estimates of Campanian pCO_2	Uncertainty in estimates of Campanian pCO_2 (filtered through resulting differences in Campanian climate, see above) could result in over or underestimates of CAMOH elevation (Poulsen and Jeffery, 2011). Although recent estimates for pCO_2 continue to suggest a broad range of possibilities for the Late Cretaceous ($\sim$0–3000 ppm; Breecker et al., 2010), it is more likely that Campanian pCO_2 fell between $\sim$500 and 1200 ppm (Fletcher et al., 2008; Quan et al., 2009; Royer, 2010). This places our imposed concentration of 1680 ppm pCO_2 as slightly high and would result in our simulated climate being too warm and our elevation estimates for the CAMOH being too high. However, recent modeling by Beerling et al. (2011) indicates that under elevated pCO_2 similar to the range expected for the Campanian, elevated fluxes and concentrations of trace greenhouse gasses (methane, nitrous oxide, tropospheric ozone) result in increased radiative forcing of 1.7–2.3 W m^{-2}. This is similar to the radiative forcing difference of $\sim$2 W m^{-2} (Ramaswamy et al., 2001) between our specified pCO_2 of 1680 ppm and a more moderate estimate of 1120 ppm. Given that we specify modern trace greenhouse gas concentrations (Table 1) much lower than those simulated by Beerling et al. (2011) and our simulated climate agrees well with or is cooler than the available proxies indicate (see above), it seems likely that, while our greenhouse gas distribution may not exactly match that of the Campanian, our total radiative forcing and resultant climate are close to that of the Campanian and no substantial error in paleoelevation estimate is being induced by the slightly elevated pCO_2 imposed in our simulations.

is intuitively and effectively functional in terms of investigating and understanding climatic and landscape evolution of the region. We believe that both this integrated research strategy and the description of paleoelevation in terms of threshold, scale and modern analog has substantial utility for deep-time investigation of tectonic and orogenic histories.

Acknowledgments

We thank David Noone for developing and making isoCAM3 available for the simulations described here and Carmala Garzione and two anonymous reviewers for constructive comments.

References

Aschoff, J.L., Steel, R.J., 2011. Anatomy and development of a low-accommodation clastic wedge, upper Cretaceous, Cordilleran Foreland Basin, USA. Sediment. Geol. 236, 1–24.

Beerling, D.J., Fox, A., Stevenson, D.S., Valdes, P.J., 2011. Enhanced chemistry-climate feedbacks in past greenhouse worlds. Proc. Natl. Acad. Sci. 108, 9770–9775.

Bissig, T., Riquelme, R., 2010. Andean uplift and climate evolution in the southern Atacama Desert deduced from geomorphology and supergene alunite-group minerals. Earth Planet. Sci. Lett. 299, 447–457.

Bonan, G.B., Oleson, K.W., Vertenstein, M., Levis, S., Zeng, X.B., Dai, Y.J., Dickinson, R.E., Yang, Z.L., 2002. The land surface climatology of the community land model coupled to the NCAR community climate model. J. Clim. 15, 3123–3149.

Breecker, D.O., Sharp, Z.D., McFadden, L.D., 2010. Atmospheric CO_2 concentrations during ancient greenhouse climates were similar to those predicted for A.D. 2100. Proc. Natl. Acad. Sci. 107, 576–580.

Broccoli, A.J., Manabe, S., 1992. The effects of orography on midlatitude northern hemisphere dry climates. J. Clim. 5, 1181–1201.

Burchfiel, B.C., Davis, G.A., 1972. Structural framework and evolution of the southern part of the Cordilleran orogen, western United States. Am. J. Sci. 272, 97–118.

Chamberlain, C.P., Poage, M.A., Craw, D., Reynolds, R.C., 1999. Topographic development of the Southern Alps recorded by the isotopic composition of authigenic clay minerals, South Island, New Zealand. Chem. Geol. 155, 279–294.

Cochran, J.K., Landman, N.H., Turekian, K.K., Michard, A., Schrag, D.P., 2003. Paleoceanography of the Late Cretaceous (Maastrichtian) Western Interior Seaway of North America: evidence from Sr and O isotopes. Palaeogeogr. Palaeoclimatol. Palaeoecol. 191, 45–64.

Collins, W.D., Rasch, P.J., Boville, B.A., Hack, J.J., McCaa, J.R., Williamson, D.L., Briegleb, B.P., Bitz, C.M., Lin, S.J., Zhang, M.H., 2006. The formulation and atmospheric simulation of the Community Atmosphere Model version 3 (CAM3). J. Clim. 19, 2144–2161.

Crowley, B.E., Koch, P.L., Davis, E.B., 2008. Stable isotope constraints on the elevation history of the Sierra Nevada Mountains, California. Geol. Soc. Am. Bull. 120, 588–598.

Currie, B.S., 2002. Structural configuration of the early Cretaceous Cordilleran Foreland-basin system and Sevier thrust belt, Utah and Colorado. J. Geol. 110, 697–718.

Dansgaard, W., 1964. Stable isotopes in precipitation. Tellus 16, 436–468.

Davis, S.J., Mulch, A., Carroll, A.R., Horton, T.W., Chamberlain, C.P., 2009. Paleogene landscape evolution of the central North American Cordillera: developing topography and hydrology in the Laramide foreland. Geol. Soc. Am. Bull. 121, 100–116.

Davis, S.J., Wiegand, B.A., Carroll, A.R., Chamberlain, C.P., 2008. The effect of drainage reorganization on paleoaltimetry studies: an example from the Paleogene Laramide foreland. Earth Planet. Sci. Lett. 275, 258–268.

DeCelles, P.G., 2004. Late Jurassic to Eocene evolution of the Cordilleran thrust belt and foreland basin system, western U.S.A. Am. J. Sci 304, 105–168.

DeCelles, P.G., Coogan, J.C., 2006. Regional structure and kinematic history of the Sevier fold-and-thrust belt, central Utah. Geol. Soc. Am. Bull. 118, 841–864.

Dettman, D.L., Lohmann, K., 2000. Oxygen isotope evidence for high-altitude snow in the laramide Rocky Mountains of North America during the Late Cretaceous and Paleogene. Geology 28, 243–246.

Drummond, C.N., Wilkinson, B.H., Lohmann, K.C., 1996. Climatic control of fluvial-lacustrine cyclicity in the Cretaceous Cordilleran Foreland Basin, western United States. Sedimentology 43, 677–689.

Ehlers, T.A., Poulsen, C.J., 2009. Influence of Andean uplift on climate and paleoaltimetry estimates. Earth Planet. Sci. Lett. 281, 238–248.

Elison, M.W., 1991. Intracontinental contraction in western North America: continuity and episodicity. Geol. Soc. Am. Bull. 103, 1226–1238.

Fisher, C.G., Arthur, M.A., 2002. Water mass characteristics in the Cenomanian US Western Interior seaway as indicated by stable isotopes of calcareous organisms. Palaeogeogr. Palaeoclimatol. Palaeoecol. 188, 189–213.

Fletcher, B.J., Brentnall, S.J., Anderson, C.W., Berner, R.A., Beerling, D.J., 2008. Atmospheric carbon dioxide linked with Mesozoic and early Cenozoic climate change. Nat. Geosci. 1, 43–48.

Fricke, H.C., Foreman, B.Z., Sewall, J.O., 2010. Integrated climate model-oxygen isotope evidence for a North American monsoon during the Late Cretaceous. Earth Planet. Sci. Lett. 289, 11–21.

Friedrich, A.M., Bartley, J.M., 2003. Three-dimensional structural reconstruction of a thrust system overprinted by postorogenic extension, Wah Wah thrust zone, southwestern Utah. Geol. Soc. Am. Bull. 115, 1473–1491.

Galewsky, J., 2009. Orographic precipitation isotopic ratios in stratified atmospheric flows: implications for paleo-elevation studies. Geology 37, 791–794.

Garzione, C.N., Quade, J., DeCelles, P.G., English, N.B., 2000. Predicting paleoelevation of Tibet and the Himalaya from d^{18}O vs. altitude gradients of meteoric water across the Nepal Himalaya. Earth Planet. Sci. Lett. 183, 215–229.

Garzione, C.N., Hoke, G.D., Libarkin, J.C., Withers, S., MacFadden, B.J., Eiler, J.M., Ghosh, P., Mulch, A., 2008. Rise of the Andes. Science 320, 1304–1307.

Gat, J.R., 1996. Oxygen and hydrogen isotopes in the hydrologic cycle. Annu. Rev. Earth Planet. Sci. 24, 225–262.

Gregory, K.M., Chase, C.G., 1992. Tectonic significance of paleobotanically estimated climate and altitude of the late Eocene erosion surface, Colorado. Geology 20, 581–585.

He, S., Kyser, T.K., Caldwell, W.G.E., 2005. Paleoenvironment of the Western Interior Seaway inferred from δ^{18}O and δ^{13}C values of molluscs from the Cretaceous Bearpaw marine cyclothem. Palaeogeogr. Palaeoclimatol. Palaeoecol. 217, 67–85.

Hough, B.G., Garzione, C.N., Wang, Z., Lease, R.O., Burbank, D.W., Yuan, D., 2011. Stable isotope evidence for topographic growth and basin segmentation: implications for the evolution of the NE Tibetan Plateau. Geol. Soc. Am. Bull. 123, 168–185.

Hren, M.T., Pagani, M., Erwin, D.M., Brandon, M., 2010. Biomarker reconstruction of the early Eocene paleotopography and paleoclimate of the northern Sierra Nevada. Geology 38, 7–10.

Hudec, M.R., Davis, G.A., 1989. Out-of-sequence thrust faulting and duplex formation in the Lewis thrust system, Spot Mountain, southeastern Glacier National Park, Montana. Can. J. Earth Sci. 26, 2356–2364.

IAEA/WMO, 2006. Global network of isotopes in precipitation. The GNIP Database. Accessible from: 〈http://www.isohis.iaea.org〉.

Insel, N., Poulsen, C.J., Ehlers, T.A., Sturm, C., 2012. Response of meteoric δ^{18}O to surface uplift—implications for Cenozoic Andean Plateau growth. Earth Planet. Sci. Lett. 317–318, 262–272.

Jeffrey, M.L., Poulsen, C.J., Ehlers, T.A., 2012. Impacts of Cenozoic global cooling, surface uplift, and an inland seaway on South American paleoclimate and precipitation δ^{18}O. Geol. Soc. Am. Bull. 124, 335–351.

Kent-Corson, M.L., Ritts, B.D., Zhuang, G., Bovet, P.M., Graham, S.A., Chamerlain, C.P., 2009. Stable isotopic constraints on the tectonic, topographic, and climatic evolution of the northern margin of the Tibetan Plateau. Earth Planet. Sci. Lett. 282, 158–166.

Kent-Corson, M.L., Sherman, L.S., Mulch, A., Chamberlain, C.P., 2006. Cenozoic topographic and climatic response to changing tectonic boundary conditions in Western North America. Earth Planet. Sci. Lett. 252, 453–466.

Kohn, M., Dettman, D.L., 2007. Paleoaltimetry from stable isotope compositions of fossils. In: Kohn, M. (Ed.), Paleoaltimetry: Geochemical and thermodynamic approaches. Reviews in Mineralogy and Geochemistry, vol. 66. Mineralogical Society of America, Chantilly, VA, USA, pp. 119–154.

Kohn, M.J., Miselis, J.L., Fremd, T.J., 2002. Oxygen isotope evidence for progressive uplift of the Cascade Range, Oregon. Earth Planet. Sci. Lett. 204, 151–165.

Markwick, P.J., 1998. Fossil crocodilians as indicators of Late Cretaceous and Cenozoic climates: implications for using palaeontological data in reconstructing palaeoclimate. Palaeogeogr. Palaeoclimatol. Palaeoecol. 137, 205–271.

Mathieu, R.D., Pollard, D., Cole, J.E., White, J.W.C., Webb, R.S., Thompson, S.L., 2002. Simulation of stable water isotope variations by the GENESIS GCM for modern conditions. J. Geophys. Res., 107, http://dx.doi.org/10.1029/2001JD900255.

Molnar, P., 2010. Deuterium and oxygen isotopes, paleoelevations of the Sierra Nevada, and Cenozoic climate. Geol. Soc. Am. Bull. 122, 1106–1115.

Molnar, P., England, P., 1990. Late Cenozoic uplift of mountain ranges and global climate change: chicken or egg? Nature 346, 29–34.

Mulch, A., Graham, S.A., Chamberlain, C.P., 2006. Hydrogen isotopes in Eocene river gravels and paleoelevation of the Sierra Nevada. Science 313, 87–89.

Mulch, A., Uba, C.E., Strecker, M.R., Schoenberg, R., Chamberlain, C.P., 2010. Late Miocene climate variability and surface elevation in the central Andes. Earth Planet. Sci. Lett. 290, 173–182.

Noone, D., 2003. Water isotopes in CCSM for studying water cycles in the climate system. In: Proceedings of the 8th Annual CCSM Workshop, Breckenridge, Colorado.

Noone, D., Simmonds, I., 2002. Associations between d18O of water and climate parameters in a simulation of atmospheric circulation for 1979–95. J. Clim. 15, 3150–3169.

Noone, D., Sturm, C., 2010. Comprehensive dynamical models of global and regional water isotope distributions. In: West, J., Bowen, G., Dawson, T., Tu, K. (Eds.), Isoscapes: Understanding Movement, Patterns, and Process on Earth through Isotope Mapping. Springer, Dordrecht Heidelberg, London New York, pp. 195–219.

Oleson, K.W., Dai, Y., Bonan, G., Bosilovich, M., Dickinson, R., Dirmeyer, P., Hoffman, F., Houser, P., Levis, S., Niu, G.Y., Thornton, P., Vertenstein, M., Yang, Z.L., Zeng, X., 2004. Technical description of the Community Land Model (CLM). NCAR/TN-461+STR, 186 p.

Otto-Bliesner, B.L., Brady, E.C., Shields, C., 2002. Late Cretaceous ocean: coupled simulations with the National Center for Atmospheric Research Climate System Model. J. Geophys. Res.-Atmos. 107 (10) 1029/2001JD000821.

Poage, M.A., Chamberlain, C.P., 2001. Empirical relationships between elevation and the stable isotope composition of precipitation and surface waters: considerations for studies of paleoelevation change. Am. J. Sci. 301, 1–15.

Poage, M.A., Chamberlain, C.P., 2002. Stable isotopic evidence for a pre-middle Miocene rain shadow in the western Basin and Range: implication for the paleo-topography of the Sierra Nevada. Tectonics, 21, http://dx.doi.org/10.1029/2001TC001303.

Poulsen, C.J., Ehlers, T.A., Insel, N., 2010. Onset of convective rainfall during gradual late Miocene rise of the Central Andes. Science 328, 490–493.

Poulsen, C.J., Jeffery, M.L., 2011. Climate change imprinting on stable isotopic compositions of high-elevation meteoric water cloaks past surface elevations of major orogens. Geology 39, 595–598, http://dx.doi.org/10.1130/G32052.1.

Quan, C., Sun, C., Sun, Y., Sun, G., 2009. High resolution estimates of paleo-CO_2 levels through the Campanian (Late Cretaceous) based on *Ginkgo* cuticles. Cretac. Res. 30, 424–428.

Ramaswamy, V., et al., 2001. Radiative forcing of climate change. In: Houghton, J.T., Ding, Y., Griggs, D.J., Noguer, M., van der Linden, P.J., Da, X., Maskell, K., Johnson, C.A. (Eds.), Climate Change 2001: The Scientific Basis. Contribution of Working Group I to the Third Assessment Report of The Intergovernmental Panel on Climate Change. Cambridge University Press, Cambridge, United Kingdom and New York, NY, USA, pp. 349–416.

Reiners, P.W., Ehlers, T.A., Mitchell, S.G., Montgomery, D.R., 2003. Coupled spatial variations in precipitation and long-term erosion rates across the Washington Cascades. Nature 426, 645–647.

Roberts, L.N.R., Kirschbaum M.A., 1995. Paleogeography of the Late Cretaceous of the Western Interior of Middle North America—coal distribution and sediment accumulation. United States Geological Survey, Professional Paper 1561, 115 p.

Roberts, E.M., 2007. Facies architecture and depositional environments of the Upper Cretaceous Kaiparowits Formation, southern Utah. Sediment. Geol. 197, 207–233.

Rowley, D.B., Pierrehumbert, R.T., Currie, B.S., 2001. A new approach to stable isotope-based paleoaltimetry: implications for paleoaltimetry and paleohypsometry of the High Himalaya since the Late Miocene. Earth Planet. Sci. Lett. 188, 253–268.

Royer, D.L., 2010. Fossil soils constrain ancient climate sensitivity. Proc. Natl. Acad. Sci. 107, 517–518.

Rozanski, K., Araguás-Araguás, L., Gonfiantini, R., 1993. Isotopic patterns in modern global precipitation. In: Swart, P.K., Lohmann, K.C., McKenzie, J., Savings, S. (Eds.), Climate Change in the Continental Isotopic Records. American Geophysical Union, Washington, DC, USA, pp. 1–36.

Ruddiman, W.F., Kutzbach, J.E., 1989. Forcing of late Cenozoic Northern Hemisphere climate by plateau uplift in southern Asia and the American west. J. Geophys. Res.-Atmos. 94, 18409–18427.

Ruddiman, W.F., Kutzbach, J.E., 1990. Late Cenozoic plateau uplift and climate change. Trans. R. Soc. Edinburgh Earth Sci. 81, 301–314.

Saward, S.A., 1992. A global view of Cretaceous vegetation patterns. In: McCabe, P.J., Parrish, J.T. (Eds.), Controls on the Distribution and Quality of Cretaceous Coals. Geological Society of America Special Paper 267. Geological Society of America, pp. 17–35.

Sewall, J.O., van de Wal, R.S.W., van der Zwan, K., van Oosterhout, C., Dijkstra, H.A., Scotese, C.R., 2007. Climate model boundary conditions for four Cretaceous time slices. Clim. Past 3, 647–657.

Snell, K.E., 2011. Paleoclimate and paleoelevation of the western Cordillera in the United States. Ph.D. Dissertation. University of California at Santa Cruz, Santa Cruz, California, 213 p.

Snell, K.E., Thrasher, B.L., Eiler, J.M., Koch, P.L., Sloan, L.C., Tabor, N.J. Hot summers in the Bighorn Basin during the early Paleogene. Geology, G33567, http://dx.doi.org/10.1130/G33567.1, in press.

Speelman, E.N., Sewall, J.O., Noone, D., Huber, M., von der Heydt, A., Sinninghe Damsté, J., Reichart, G.-J., 2010. Modeling the influence of a reduced equator-to-pole temperature gradient on the distribution of water isotopes in the Early/Middle Eocene. Earth Planet. Sci. Lett. 298, 57–65.

Straight, W.H., Barrick, R.E., Eberth, D.A., 2004. Reflections of surface water, seasonality, and climate in stable oxygen isotopes from tyrannosaurid tooth enamel. Palaeogeogr. Palaeoclimatol. Palaeoecol. 206, 239–256.

Vakhrameev, V.A., 1991. Jurassic and Cretaceous Floras and Climate of the Earth. Cambridge University Press, Cambridge, Great Britain 269.

Weil, A.B., Yonkee, A., Sussman, A., 2010. Reconstructing the kinematic evolution of curved mountain belts: a paleomagnetic study of Triassic red beds from the Wyoming salient, Sevier thrust belt, USA. Geol. Soc. Am. Bull. 122, 3–23.

Wobus, C.W., Hodges, K.V., Whipple, K.X., 2003. Has focused denudation sustained active thrusting at the Himalayan topographic front? Geology 31, 861–864.

Wolfe, J.A., Forest, C.E., Molnar, P., 1998. Paleobotanical evidence of Eocene and Oligocene paleoaltitudes in midlatitude western North America. Geol. Soc. Am. Bull. 110, 664–678.

Wolfe, J.A., Upchurch Jr., G.R., 1987. North American nonmarine climates and vegetation during the Late Cretaceous. Palaeogeogr. Palaeoclimatol. Palaeoecol. 61, 33–77.

Zaleha, M.J., 2006. Sevier orogenesis and nonmarine basin filling: implications of new stratigraphic correlations of Lower Cretaceous strata throughout Wyoming. Geol. Soc. Am. Bull. 118, 886–896.

Zhou, J., Poulsen, C.P., Pollard, D., White, T.S., 2008. Simulation of modern and middle Cretaceous marine $\delta^{18}O$ with an ocean–atmosphere general circulation model. Paleoceanography, 23, http://dx.doi.org/10.1029/2008PA001596.